RESEARCH　　　　　　　　　　　　　　　　　　　　**Open Access**

CrossMark

Effects of radiation on MHD free convection of a Casson fluid from a horizontal circular cylinder with partial slip in non-Darcy porous medium with viscous dissipation

Gilbert Makanda[*], Sachin Shaw and Precious Sibanda

[*]Correspondence:
gilbertmakanda@yahoo.com
School of Mathematics, Statistics
and Computer Science, University
of KwaZulu-Natal, Private Bag X01,
Scottsville, Pietermaritzburg, 3209,
South Africa

Abstract

In the present study, the effects of radiation on MHD free convection from a cylinder with partial slip in a Casson fluid in non-Darcy porous medium is investigated. The surface of the cylinder is heated under constant surface temperature with partial slip. Partial slip factors are considered on the surface for both velocity and temperature. The boundary layer equations are normalized into a system of non-similar partial differential equations and are then solved using a bi-variate quasilinearization method (BQLM). The boundary layer velocity and temperature profiles are computed for different values of the physical parameters. Increasing the Forchheimer parameter decreases the temperature profiles. The decrease of the velocity profiles with the increase in magnetic parameter is more enhanced in the presence of the velocity slip factor. Increasing the Eckert number increases the temperature profiles in both suction and blowing cases. This study considers the unique problem of the effect of transpiration in a Casson fluid in the presence of radiation, a magnetic field, and viscous dissipation. The results obtained in this study are compared with other numerical methods and were found to be in excellent agreement.

Keywords: Casson fluid; partial slip; viscous dissipation; bi-variate quasilinearization method

1 Introduction

The flow of non-Newtonian fluids is applied in many situations in industry such as processing of materials and chemical engineering. These fluids show different characteristics from the Newtonian fluids which cannot be fully represented by the Navier-Stokes equations. To represent these non-Newtonian fluids some modifications to the Navier-Stokes equations are used and these are seen in many research works which studied viscoelastic and micropolar fluids [1, 2]. These fluids are categorized as viscoelastic, thixotropic, and power-law fluids. The constitutive equations of such fluids cannot fully represent the actual behavior of these fluids. These fluids include contaminated lubricants, molten metal, synovial fluids, *etc.*

The study of radiation effects on MHD free convection of a Casson fluid in porous medium with partial slip is an important aspect due to its practical application in the

design of automatic cooking machines and the design of internal engine parts in mechanical engineering. Other examples arise in petroleum production, multiphase mixtures, pharmaceutical formulations, coal in water, paints, lubricants, jams, sewage, soup, blood. There has been a significant improvement in the study of non-Newtonian fluids in which many different situations have been considered. Studies in a Casson fluid include work by among others Mukhopadhyay *et al.* [3] and Nadeem *et al.* [4].

Several research workers have studied radiation effects, these include Kameswaran *et al.* [5] who studied radiation effects on hydromagnetic Newtonian liquid flow due to an exponentially stretching sheet. They studied radiation effects in the presence of a magnetic field, advancing the studies of radiation effects in Newtonian fluids. Shateyi and Marewo [6] investigated numerical analysis of MHD stagnation point flow of a Casson fluid, they considered thermal radiation in their work. Chamkha *et al.* [7] studied thermal radiation effects on MHD forced convection flow adjacent to a non-isothermal wedge in the presence of a heat source or sink. Pramanik [8] studied Casson fluid flow and heat transfer past an exponentially porous stretching surface in the presence of thermal radiation.

The study of fluid flow in the presence of a magnetic fluid has also been performed by many authors, among others Ece [9], who investigated free convection flow about a cone under mixed thermal boundary conditions and a magnetic field. Narayana *et al.* [10] studied free magnetohydrodynamic flow and convection from a vertical spinning cone with cross diffusion effects. Nadeem *et al.* [11] studied numerically MHD boundary layer flow of a Maxwell fluid past a stretching sheet in the presence of nanoparticles. Chen [12] investigated the combined heat and mass transfer in MHD free convection from a vertical surface with ohmic heating and viscous dissipation.

The study of fluid flow past a cylindrical geometry was performed by among others Anwa *et al.* [13], who studied mixed convection boundary layer flow of a viscoelastic fluid over a horizontal cylinder. Deka *et al.* [14] investigated transient free convection flow past an accelerated vertical cylinder in a rotating cylinder. Ribeiro *et al.* [15] studied viscoelastic flow past a confined cylinder with three dimensional effects and stability. Patel and Chhabra [16] studied steady flow of Bingham plastic fluids past an elliptical cylinder.

Studies in porous media and viscous dissipation have been carried out by among others, Awad *et al.* [17] who studied natural convection of viscoelastic fluid from a cone embedded in a porous medium with viscous dissipation. Awad *et al.* [17] investigated convection from an inverted cone in a porous medium with cross diffusion effects. Hayat *et al.* [18] studied heat and mass transfer for Soret and Dufour effects on mixed convection boundary layer flow over a stretching vertical surface in a porous medium filled with a viscoelastic fluid. Cheng [19] studied Soret and Dufour effects on free convection boundary layer over a vertical cylinder in a saturated porous medium. Chamkha and Rashad [20] investigated natural convection from a vertical permeable cone in nanofluid saturated porous media for uniform heat and nanoparticles volume fraction fluxes.

In this study we investigate the effects of radiation in MHD free convection of a Casson fluid from a horizontal circular cylinder with partial slip in non-Darcy porous medium with viscous dissipation. The surface of the cylinder is perforated in which we have the effects of transpiration which acts transversely in the direction ξ. The force which causes transpiration is sometimes called the Forchheimer drag force term $-\xi \Lambda f'^2$, which appears in the momentum equation (12). This term is also associated with the geometry of the porous medium. In this work we extended the work of Ramachandra *et al.* [1] in which we

introduced magnetic field, radiation effects and viscous dissipation. We also solved the system of the resulting partial differential equations by the bi-variate quasilinearization method (BQLM). The method is described in detail in Motsa *et al.* [21]. We study the effects of the magnetic field, radiation. and the Eckert number on velocity and temperature profiles for different values of the Casson parameter β, the local inertia (Forchheimer parameter) Λ, and the Darcian drag force coefficient Λ_1. The results of this work are validated by comparison with other methods, which are the successive linearization method (SLM) and MATLAB's routine 'bvp4c'.

2 Mathematical formulation

The steady, laminar, two dimensional MHD free convection of a Casson fluid flow from a horizontal circular cylinder with partial slip in a non-Darcy porous medium, with viscous dissipation and radiation effects, is considered. The fluid is maintained at a uniform temperature T_w ($> T_\infty$), the transpiration velocity V_w is in the direction ξ. x is the tangential coordinate of the circle and y is the radial coordinate of the circle. u and v are the velocity components in the x and y directions, respectively, as shown in Figure 1.

The rheological equation of state for an isotropic and incompressible flow of a Casson fluid is given as in [1–3] by

$$\tau_{ij} = \begin{cases} 2(\mu_B + \frac{P_y}{\sqrt{2\pi}})e_{ij}, & \pi > \pi_c, \\ 2(\mu_B + \frac{P_y}{\sqrt{2\pi_c}})e_{ij}, & \pi < \pi_c, \end{cases} \tag{1}$$

$\pi = e_{ij}e_{ij}$ and e_{ij} is the (i,j)th component of the deformation rate, π is the product of the deformation rate with itself, π_c is a critical value of this product based on the non-Newtonian model, μ_B is the plastic dynamic viscosity of the non-Newtonian fluid, P_y is the yield stress of the fluid.

The governing equations in this flow are given as

$$\frac{\partial}{\partial x}(ru) + \frac{\partial}{\partial y}(rv) = 0, \tag{2}$$

$$u\frac{\partial u}{\partial x} + v\frac{\partial u}{\partial y} = v\left(1 + \frac{1}{\beta}\right)\frac{\partial^2 u}{\partial y^2} + \bar{g}\beta_T(T - T_\infty)\sin\left(\frac{x}{a}\right) - \Gamma u^2 - \frac{v}{\bar{K}}u - \frac{\sigma B_0^2}{\rho}u, \tag{3}$$

$$u\frac{\partial T}{\partial x} + v\frac{\partial T}{\partial y} = \alpha\frac{\partial^2 T}{\partial y^2} - \frac{1}{\rho C_p}\frac{\partial q_r}{\partial y} + \frac{v}{\rho C_p}\left(1 + \frac{1}{\beta}\right)\left(\frac{\partial u}{\partial y}\right)^2 + \frac{\sigma B_0^2 u^2}{\rho C_p}, \tag{4}$$
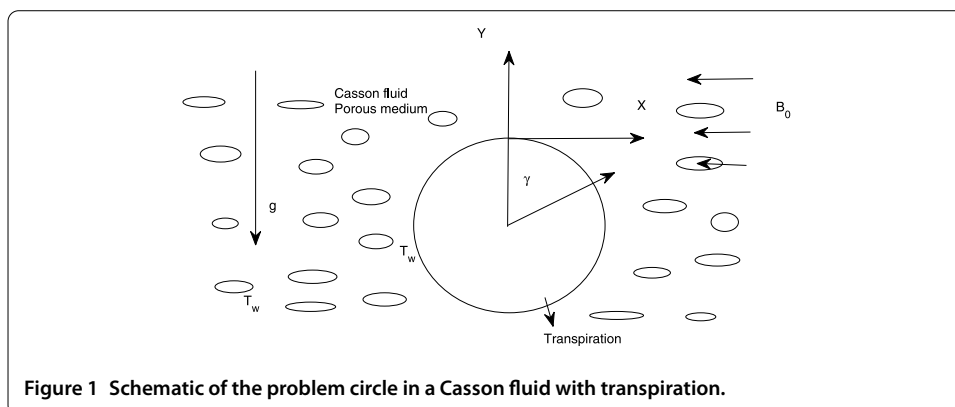

Figure 1 Schematic of the problem circle in a Casson fluid with transpiration.

where u and v are the velocity components in the x and y directions, respectively, a is the radius of the cylinder, v is the kinematic viscosity of the Casson fluid, $\beta = \mu_B \sqrt{2\pi_c}/P_y$ is the non-Newtonian Casson parameter, $\alpha = \kappa/\rho C_p$ is the thermal diffusivity, κ is thermal conductivity of the fluid, q_r is the radiative heat flux, C_p is the specific heat, $\bar{g}$ is the acceleration due to gravity, β_T is the coefficient of thermal expansions, and T is the temperature of the fluid. T_∞ is the free stream temperature, ρ is the fluid density, $\bar{K}$ and Γ are the permeability and inertia coefficients respectively. σ is the electric conductivity and B_0 is the magnetic flux density. The Rosseland approximation for radiation may be written as follows:

$$q_r = -\frac{4\sigma^*}{3k^*}\frac{\partial T^4}{\partial y},$$
(5)

where σ^* is the Stefan-Boltzmann constant and k^* is the absorption coefficient. If the temperature difference within the flow is such that T^4 may be expanded in a Taylor series about T_∞ and neglecting higher powers, we obtain $T^4 - 4T_\infty^3 - 3T_\infty^4$ and therefore (4) can be written as

$$u\frac{\partial T}{\partial x} + v\frac{\partial T}{\partial y} = \alpha\frac{\partial^2 T}{\partial y^2} + \frac{16\sigma^* T_\infty^3}{3\rho C_p k^*}\frac{\partial^2 T}{\partial y^2} + \frac{v}{\rho C_p}\left(1 + \frac{1}{\beta}\right)\left(\frac{\partial u}{\partial y}\right)^2 + \frac{\sigma B_0^2 u^2}{\rho C_p}.$$
(6)

The boundary conditions are given as

$$u = N_0\left(1 + \frac{1}{\beta}\right)\frac{\partial u}{\partial y}, \qquad v = -V_w, \qquad T = T_w + K_0\frac{\partial T}{\partial Y}, \qquad y = 0,$$
(7)

$$u \to 0, \qquad T \to T_\infty, \quad \text{as } y \to \infty,$$
(8)

where N_0 is the velocity slip factor, K_0 is the thermal slip factor. $N_0 = K_0 = 0$ corresponds to no-slip conditions. The subscripts w and ∞ refer to surface and ambient conditions, respectively.

We introduce the non-dimensional variables

$$\left.\begin{array}{l}
\xi = \dfrac{x}{a}, \qquad \eta = \dfrac{y}{a}Gr^{\frac{1}{4}}, \qquad Pr = \dfrac{v}{\alpha}, \\[2mm]
Gr = \dfrac{g\beta_T(T_w - T_\infty)a^3}{v^2}, \qquad \beta_c = \mu_B\dfrac{\sqrt{2\pi_c}}{P_y}, \\[2mm]
\Lambda = \Gamma a, \qquad \Lambda_1 = \dfrac{1}{DaGr^{\frac{1}{2}}}, \qquad Da = \dfrac{\bar{K}}{a^2}, \qquad f_w = -\dfrac{V_w a}{vGr^{\frac{1}{4}}}, \qquad U_0 = \dfrac{vGr^{\frac{1}{2}}}{a}.
\end{array}\right\}$$
(9)

Introducing the stream function ψ and similarity variables

$$u = \frac{\partial \psi}{\partial y} \quad \text{and} \quad v = -\frac{\partial \psi}{\partial x},$$
(10)

$$f(\xi, \eta) = \frac{\psi}{v\xi Gr^{\frac{1}{4}}}, \qquad \theta(\xi, \eta) = \frac{T - T_\infty}{T_w - T_\infty},$$
(11)

using the stream function defined in (10) and the similarity variable in (11), (2)-(6) together with the boundary conditions (7) and (8) reduce to the following system of partial

differential equations:

$$\left(1 + \frac{1}{\beta}\right)f''' + ff'' - (1 + \Lambda\xi)f'^2 - \left(\Lambda_1 + M^2\right)f' + \frac{\sin(\xi)}{\xi}\theta = \xi\left(f'\frac{\partial f'}{\partial\xi} - f''\frac{\partial f}{\partial\xi}\right), \tag{12}$$

$$\frac{1}{Pr}\left(1 + \frac{4}{3}K\right)\theta'' + f\theta' + \xi^2 Ec\left[\left(1 + \frac{1}{\beta}\right)f''^2 + M^2(f')^2\right] = \xi\left(f'\frac{\partial\theta}{\partial\xi} - \theta'\frac{\partial f}{\partial\xi}\right) \tag{13}$$

with boundary conditions

$$\eta = 0, \qquad f = f_w, \qquad f' = \left(1 + \frac{1}{\beta}\right)S_f f'', \qquad \theta = 1 + S_T \theta', \tag{14}$$

$$\eta \to \infty, \qquad f' \to 0, \qquad \theta \to 0, \tag{15}$$

where β is the Casson parameter, Λ is the Forchheimer parameter, Λ_1 is the Darcian drag coefficient, M is the magnetic field parameter, K is the radiation parameter, Pr is the Prandtl number, Ec is the Eckert number, $f_w > 0$ corresponds to suction, and $f_w < 0$ corresponds to blowing, $S_f = N_0 Gr^{\frac{1}{4}}/L$ is the velocity slip factor, and $S_T = kGr^{\frac{1}{4}}/L$ is the thermal slip factor. In the above equations the primes refer to the derivative with respect to η. The engineering parameters of interest are the local skin friction and the local Nusselt numbers, which are defined as follows.

The shear stress at the surface of the cone is given by

$$\tau_w = \mu\left[\left(1 + \frac{1}{\beta}\right)\frac{\partial u}{\partial y}\right]_{y=0} = \frac{\mu(1 + \frac{1}{\beta})\nu\xi Gr^{\frac{3}{4}}}{a^2}f''(0), \tag{16}$$

where μ is the coefficient of viscosity. The skin friction coefficient is given by

$$C_f = \frac{\tau_w}{\frac{1}{2}\rho U_0^2}. \tag{17}$$

Using (16) and (17) together with (10) and (11) give

$$C_f Gr^{-\frac{3}{4}} = \left(1 + \frac{1}{\beta}\right)\xi f''(0). \tag{18}$$

The heat transfer from the surface of the circle into the fluid is given by

$$q_w = -k\left[\frac{\partial T}{\partial y}\right]_{y=0} = \frac{-k(T_w - T_\infty)}{aGr^{-\frac{1}{4}}}X\theta'(0), \tag{19}$$

k is the thermal conductivity of the fluid. The Nusselt number under LST is given by

$$Nu = \frac{a}{k}\frac{q_w}{T_w - T_\infty}. \tag{20}$$

Equations (19) and (20) together with (10) and (11) give

$$NuGr^{-\frac{1}{4}} = -\theta'(0). \tag{21}$$

3 Solution method

In this section we describe the implementation of the bi-variate quasilinearization method (BQLM) which is based on the quasilinearization method (QLM) which is described in detail in Motsa *et al.* [21]. We apply the quasilinearization method (QLM) first proposed by Bellman and Kalaba [22] to (12)-(13), which is based on the Taylor series expansion with the assumption that the differences $(f_{r+1} - f_r)$, $(\theta_{r+1} - \theta_r)$, and all the derivatives are small. We obtain the following equations:

$$\left(1 + \frac{1}{\beta}\right)f'''_{r+1} + a_{1,r}(\eta,\xi)f''_{r+1} + a_{2,r}(\eta,\xi)f'_{r+1} + a_{3,r}(\eta,\xi)f_{r+1}$$

$$+ a_{4,r}(\eta,\xi)\frac{\partial f'_{r+1}}{\partial \xi} + a_{5,r}(\eta,\xi)\frac{\partial f_{r+1}}{\partial \xi} = a_{6,r}(\eta,\xi), \tag{22}$$

$$\frac{1}{Pr}\left(1 + \frac{4}{3}K\right)\theta''_{r+1} + b_{1,r}(\eta,\xi)\theta'_{r+1} + b_{2,r}(\eta,\xi)\frac{\partial \theta_{r+1}}{\partial \xi} = b_{3,r}(\eta,\xi), \tag{23}$$

where

$$a_{1,r} = f_r + \xi\frac{\partial f_r}{\partial \xi}, \tag{24}$$

$$a_{2,r} = -\left[2(1 + \Lambda\xi)f'_r + \Lambda_1 + M^2 + \xi\frac{\partial f'_r}{\partial \xi}\right], \tag{25}$$

$$a_{3,r} = f''_r, \tag{26}$$

$$a_{4,r} = -\xi f'_r, \tag{27}$$

$$a_{5,r} = \xi f''_r, \tag{28}$$

$$a_{6,r} = f_r f''_r - (1 + \Lambda\xi)(f'_r)^2 - \frac{\sin\xi}{\xi}\theta_r - \xi\left(\frac{\partial f'_r}{\partial \xi} - f''_r\frac{\partial f_r}{\partial \xi}\right), \tag{29}$$

$$b_{1,r} = f_r + \xi\frac{\partial f_r}{\partial \xi}, \tag{30}$$

$$b_{2,r} = -\xi f'_r, \tag{31}$$

$$b_{3,r} = -Ec\xi^2\left[\left(1 + \frac{1}{\beta}\right)(f''_r)^2 + M^2(f'_r)^2\right]. \tag{32}$$

The solution for the now linear partial differential equations (22)-(23) is obtained by approximating the exact solutions of $f(\eta,\xi)$ and $\theta(\eta,\xi)$ by the Lagrange form of polynomial $F(\eta,\xi)$ and $\Theta(\eta,\xi)$ at the selected collocation points,

$$0 = \xi_0 < \xi_1 < \xi_2 < \cdots < \xi_{N_\xi} = 1.$$

The approximation for $f(\eta,\xi)$ and $\theta(\eta,\xi)$ has the form

$$f(\eta,\xi) \approx \sum_{j=0}^{N_\xi} F(\eta,\xi)L_j(\xi) = \sum_{j=0}^{N_\xi} F_j(\eta)L_j(\xi), \tag{33}$$

$$\theta(\eta,\xi) \approx \sum_{j=0}^{N_\xi} \Theta(\eta,\xi)L_j(\xi) = \sum_{j=0}^{N_\xi} \Theta_j(\eta)L_j(\xi), \tag{34}$$

where $F_j(\eta) = F(\eta, \xi)$ and $\Theta_j(\eta) = \Theta(\eta, \xi)$, L_j is the characteristic Lagrange cardinal polynomial defined as

$$L_j(\xi) = \prod_{k=0, k \neq j}^{M} \frac{\xi - \xi_k}{\xi_j - \xi_k}, \tag{35}$$

which obey the Kronecker delta equation

$$L_j(\xi_k) = \delta_{jk} = \begin{cases} 0 & \text{if } j \neq k, \\ 1 & \text{if } j = k. \end{cases} \tag{36}$$

The equations for the solution of $F_j(\eta)$ and $\Theta_j(\eta)$ are obtained by substituting (33)-(34) into (22)-(23) and letting the equations be satisfied at the points ξ_i, $i = 0, 1, 2, \ldots, N_\xi$. To compute the derivatives of the Lagrange polynomial analytically we transform $\xi \in [0, L_\xi]$ to $\zeta \in [-1, 1]$, and then we choose Chebyshev-Gauss-Lobatto points $\zeta_i = \cos \frac{i\pi}{N_\xi}$. After using the linear transformation $\xi = L_\xi(\zeta + 1)/2$, the derivatives of f' with respect to the collocation points ζ_j are computed as

$$\frac{\partial f'}{\partial \xi}\bigg|_{\xi = \xi_i} = 2 \sum_{j=0}^{N_\xi} F_j'(\eta) \frac{dL_j}{d\zeta}(\zeta_i) = \sum_{j=0}^{N_\xi} \mathbf{d}_{i,j} F_j'(\eta), \quad i = 0, 1, 2, \ldots, N_\xi, \tag{37}$$

where $\mathbf{d}_{i,j} = \frac{dL_j}{d\zeta}(\zeta_i)$ $(i = 0, 1, \ldots, N_\xi)$ are entries of the standard Chebyshev differentiation matrix, $\mathbf{d} = \frac{2}{L_\xi} d$. We now apply the collocation (η, ξ_i) in (22)-(23) we obtain

$$\left(1 + \frac{1}{\beta}\right) F_{r+1,i}'''(\eta) + a_{1,r}^{(i)} F_{r+1,i}''(\eta) + a_{2,r}^{(i)} F_{r+1,i}'(\eta) + a_{3,r}^{(i)} F_{r+1,i}(\eta)$$

$$+ a_{4,r}^{(i)} \sum_{j=0}^{N_\xi} \mathbf{d}_{i,j} F_{r+1,i}'(\eta) + a_{5,r}^{(i)} \sum_{j=0}^{N_\xi} \mathbf{d}_{i,j} F_{r+1,i}(\eta) = a_{6,r}^{(i)}, \tag{38}$$

$$\frac{1}{Pr}\left(1 + \frac{4}{3}K\right) \Theta_{r+1,i}''(\eta) + b_{1,r}^{(i)} \Theta_{r+1,i}'(\eta) + b_{2,r}^{(i)} \sum_{j=0}^{N_\xi} \mathbf{d}_{i,j} \Theta_{r+1,i}(\eta) = b_{3,r}^{(i)}, \tag{39}$$

where $a_{k,r}^{(i)} = a_{k,r}(\eta, \xi_i)$ $(k = 1, 2, 3, 4, 5, 6)$ and $b_{k,r}^{(i)} = b_{k,r}(\eta, \xi_i)$ $(k = 1, 2, 3)$. Since the solution at $\xi = 0$ ($\zeta = \zeta_{N_\xi}$) is known, we evaluate (38)-(39) for $i = 0, 1, \ldots, N_\xi - 1$ and the system becomes

$$\left(1 + \frac{1}{\beta}\right) F_{r+1,i}''' + a_{1,r}^{(i)} F_{r+1,i}'' + a_{2,r}^{(i)} F_{r+1,i}' + a_{3,r}^{(i)} F_{r+1,i} + a_{4,r}^{(i)} \sum_{j=0}^{N_\xi - 1} \mathbf{d}_{i,j} F_{r+1,i}'$$

$$+ a_{5,r}^{(i)} \sum_{j=0}^{N_\xi - 1} \mathbf{d}_{i,j} F_{r+1,i} = a_{6,r}^{(i)} - a_{4,r}^{(i)} \mathbf{d}_{i,N_\xi} F_{r+1,N_\xi}' - a_{5,r}^{(i)} \mathbf{d}_{i,N_\xi} F_{r+1,N_\xi}, \tag{40}$$

$$\frac{1}{Pr}\left(1 + \frac{4}{3}K\right) \Theta_{r+1,i}'' + b_{1,r}^{(i)} \Theta_{r+1,i}' + b_{2,r}^{(i)} \sum_{j=0}^{N_\xi - 1} \mathbf{d}_{i,j} \Theta_{r+1,i}$$

$$= b_{3,r}^{(i)} - b_{2,r}^{(i)} \mathbf{d}_{i,N_\xi} \Theta_{r+1,N_\xi}. \tag{41}$$

For each ξ_i, (40)-(41) forms a system of linear ordinary differential equations with variable coefficients. In this system we apply the Chebyshev spectral collocation independently in the η direction by choosing $N_\eta + 1$ Chebyshev-Gauss-Lobatto points $0 = \eta_0 < \eta_1 < \eta_2 < \cdots < \eta_{N_\eta} = \eta_e$, where η_e is a finite value that is chosen to be adequately large to approximate the conditions at ∞. We now implement the collocation in the interval $[0, \eta_e]$ on the η-axis, which is then transformed into the interval $[-1, 1]$ using a linear transformation $\eta = \eta_e(\tau + 1)/2$. The collocation points are chosen as $\tau_j = \cos \frac{j\pi}{N_\eta}$. The derivatives with respect to η are defined in terms of the Chebyshev differentiation matrix as

$$\frac{d^p F'_{r+1,i}}{d\eta^p}\bigg|_{\eta=\eta_j} = \left(\frac{2}{\eta_e}\right)^p \sum_{k=0}^{N_\eta} D_{j,k}^p F_{r+1,i}(\tau_k) = \left[\mathbf{D}^p \mathbf{F}_{r+1,i}\right]_j, \tag{42}$$

where p is the order of the derivative, $\mathbf{D} = \frac{2}{\eta_e} D$ $(j, k = 0, 1, 2, \ldots, N_\eta)$ with D being an $(N_\eta + 1) \times (N_\eta + 1)$ Chebyshev derivative matrix, and the vector $\mathbf{F}_{r+1,i}$ is defined as

$$\mathbf{F}_{r+1,i} = \left[F_{r+1,1}(\tau_0), F_{r+1,1}(\tau_1), \ldots, F_{r+1,1}(\tau_{N_\eta})\right]^T, \tag{43}$$

$$\mathbf{\Theta}_{r+1,i} = \left[\Theta_{r+1,i}(\tau_0), \Theta_{r+1,i}(\tau_1), \ldots, \Theta_{r+1,i}(\tau_{N_\eta})\right]^T, \tag{44}$$

substituting (42) into (40) we get

$$\mathbf{A}^{(i)}\mathbf{F}_{r+1,i} + \mathbf{a}_{4,r}^{(i)} \sum_{j=0}^{N_\xi-1} d_{i,j}\mathbf{D}\mathbf{F}_{r+1,j} + \mathbf{a}_{5,r}^{(i)} \sum_{j=0}^{N_\xi-1} d_{i,j}\mathbf{F}_{r+1,j} = R_1^{(i)}, \tag{45}$$

$$\mathbf{A}^{(i)} = \left(1 + \frac{1}{\beta}\right)\mathbf{D}^3 + \mathbf{a}_{1,r}^{(i)}\mathbf{D}^2 + a_{2,r}^{(i)}\mathbf{D} + \mathbf{a}_{2,r}^{(i)}, \tag{46}$$

$$\mathbf{R}_1^{(i)} = \mathbf{a}_{6,r}^{(i)} - \mathbf{a}_{4,r}^{(i)} d_{i,N_\xi}\mathbf{D}\mathbf{F}_{r+1,N_\xi} - \mathbf{a}_{5,r}^{(i)} d_{i,N_\xi}\mathbf{F}_{r+1,N_\xi} \tag{47}$$

$$\mathbf{B}^{(i)}\mathbf{\Theta}_{r+1,i} + \mathbf{b}_{2,r}^{(i)} \sum_{j=0}^{N_\xi-1} d_{i,j}\mathbf{\Theta}_{r+1,j} = R_2^{(i)}, \tag{48}$$

$$\mathbf{B}^{(i)} = \frac{1}{Pr}\left(1 + \frac{4}{3}K\right)\mathbf{D}^2 + \mathbf{b}_{1,r}^{(i)}\mathbf{D}, \tag{49}$$

$$\mathbf{R}_2^{(i)} = \mathbf{b}_{3,r}^{(i)} - \mathbf{b}_{2,r}^{(i)} d_{i,N_\xi}\mathbf{\Theta}_{r+1,N_\xi}. \tag{50}$$

$\mathbf{a}_{k,r}$ $(k = 1, 2, 3, 4, 5, 6)$, $\mathbf{b}_{k,r}$ $(k = 1, 2, 3)$ are the diagonal matrices with vectors $[a_{k,r}(\tau_0), a_{k,r}(\tau_1), \ldots, a_{k,r}(\tau_{N_x})]^T$ and $[b_{k,r}(\tau_0), b_{k,r}(\tau_1), \ldots, b_{k,r}(\tau_{N_x})]^T$. We then impose boundary conditions and a matrix system is formed as follows:

$$\mathbf{AA} = \left(\begin{array}{cccc|cccc} A_{0,0} & A_{0,1} & \cdots & A_{0,N_\xi-1} & 0 & 0 & \cdots & 0 \\ A_{1,0} & A_{1,1} & \cdots & A_{1,N_\xi-1} & 0 & 0 & \cdots & 0 \\ \vdots & \vdots & \ddots & \vdots & \vdots & \vdots & \ddots & \vdots \\ A_{N_\xi-1,0} & A_{N_\xi-1,1} & \cdots & A_{N_\xi-1,N_\xi-1} & \vdots & \vdots & \ddots & \vdots \\ \hline 0 & 0 & \cdots & 0 & B_{0,0} & B_{0,1} & \cdots & B_{0,N_\xi-1} \\ 0 & 0 & \cdots & 0 & B_{1,0} & B_{1,1} & \cdots & B_{1,N_\xi-1} \\ \vdots & \vdots & \ddots & \vdots & \vdots & \vdots & \ddots & \vdots \\ 0 & 0 & \cdots & 0 & B_{N_\xi-1,0} & B_{N_\xi-1,1} & \cdots & B_{N_\xi-1,N_\xi-1} \end{array}\right),$$

$$\mathbf{FF} = \begin{pmatrix} \mathbf{F}_{r+1,0} \\ \mathbf{F}_{r+1,1} \\ \vdots \\ \mathbf{F}_{r+1,N_\xi-1} \\ \hline \mathbf{\Theta}_{r+1,0} \\ \mathbf{\Theta}_{r+1,1} \\ \vdots \\ \mathbf{\Theta}_{r+1,N_\xi-1} \end{pmatrix}, \qquad \mathbf{RR} = \begin{pmatrix} R_1^{(0)} \\ R_1^{(1)} \\ \vdots \\ R_1^{(N_\xi-1)} \\ \hline R_2^{(0)} \\ R_2^{(1)} \\ \vdots \\ R_2^{(N_\xi-1)} \end{pmatrix}.$$

The above system is then solved as

$$\mathbf{FF} = \mathbf{AA}^{-1}\mathbf{RR}. \tag{51}$$

We have

$$A_{i,i} = \mathbf{A}^{(i)} + a_{4,r}^{(i)} d_{i,i}\mathbf{D} + a_{5,r}^{(i)} d_{i,i},$$
$$B_{i,i} = \mathbf{B}^{(i)} + b_{2,r}^{(i)} d_{i,i}, \quad i = 0,1,\ldots,N_\xi - 1, \tag{52}$$

$$A_{i,j} = a_{4,r}^{(i)} d_{i,j}\mathbf{D} + a_{5,r}^{(i)} d_{i,j}, \quad i \neq j,$$
$$B_{i,j} = b_{2,r}^{(i)} d_{i,j}, \quad i \neq j. \tag{53}$$
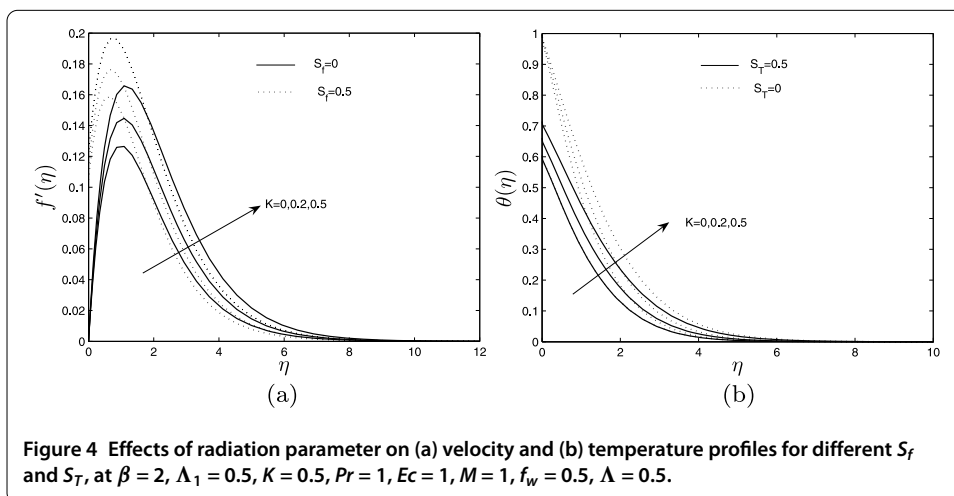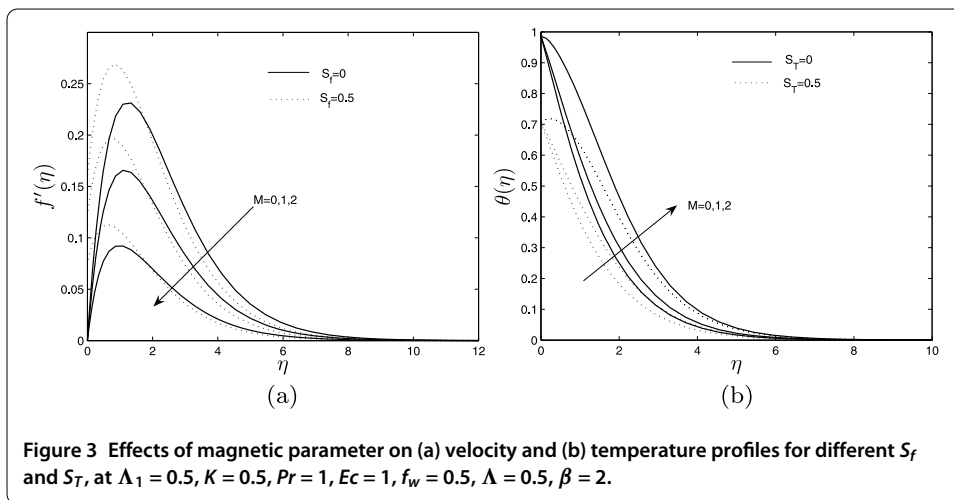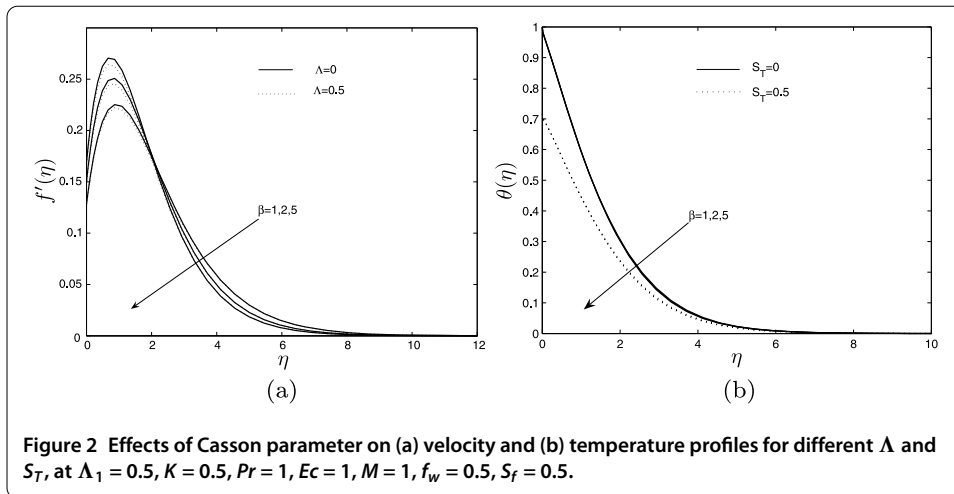
4 Results and discussion

In Table 1, we compare the results of the bi-variate quasilinearization method (BQLM) to the successive linearization method (SLM) and MATLAB's 'bvp4c' method. The results of the BQLM are in excellent agreement with these two methods to seven decimal places showing the accuracy of this method.
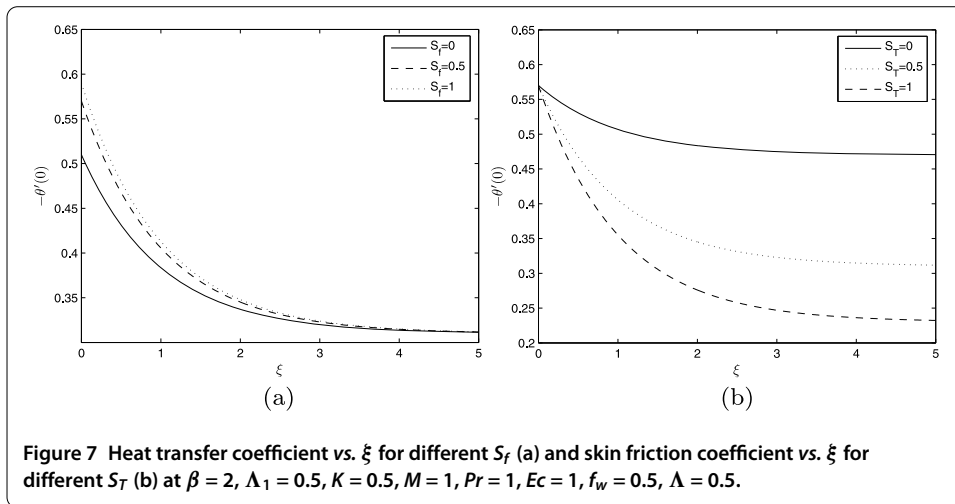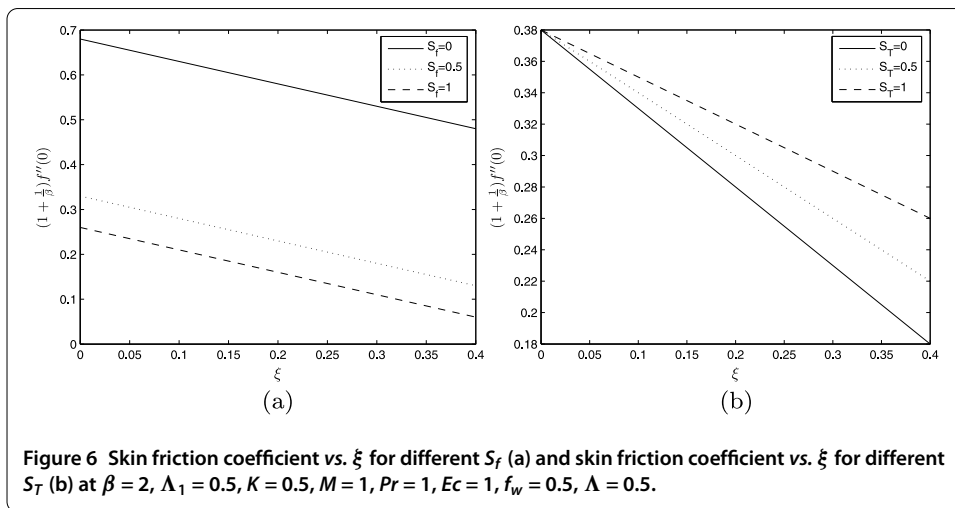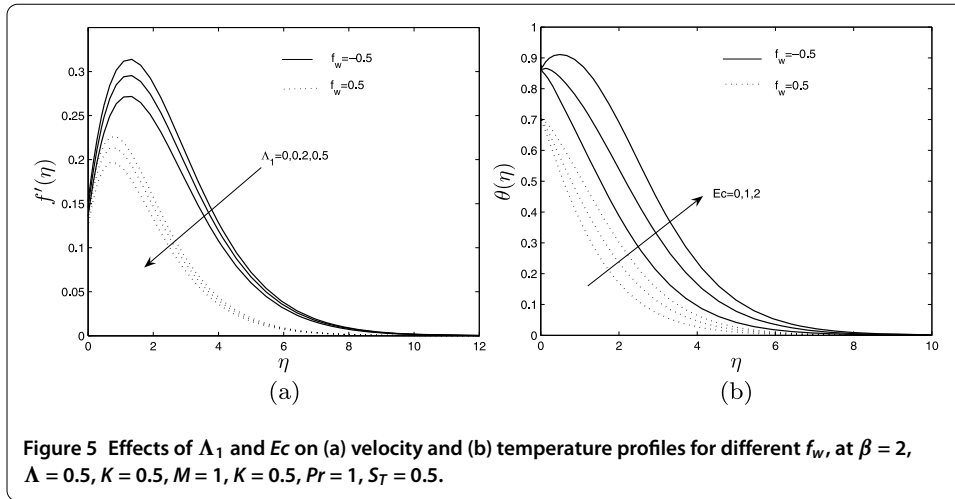
To understand the behavior of the velocity and temperature profiles the illustrations for the numerical solution obtained are depicted as graphs in Figures 2-8.
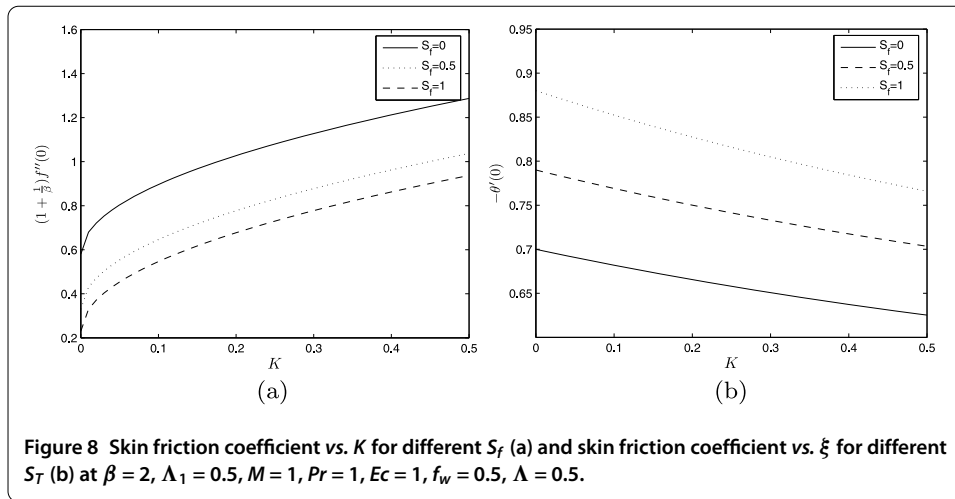
Figure 2 shows the influence of Casson parameter β on the velocity and the temperature profiles at different values of the Forchheimer parameter Λ in the case of velocity profiles (see Figure 2(a)), and thermal slip factor S_T in the case of temperature profiles (see Figure 2(b)). Increasing the Casson parameter increases the velocity profiles close to the boundary, as $\beta \to \infty$, $\frac{1}{\beta} \to 0$, the fluid becomes Newtonian. The same result is noted in Ramachandra *et al.* [1]. The difference in these results from those of Ramachandra *et al.* [1] is that there is a reverse effect that is noted further away from the boundary. This is due to the presence of the velocity slip factor which tends to assist flow at the boundary. Increasing the Forchheimer parameter reduce velocity profiles, this is caused by the transpiration effect taking place at the surface of the circle. Increasing the Casson parameter β reduces temperature profiles (see [1–3]). In the case of no thermal slip factor,

Table 1 Comparison of the values of the skin friction coefficient and heat transfer coefficient obtained by BQLM against the SLM and bvp4c for $\beta \to \infty$, $\Lambda = \Lambda_1 = M = \xi = K = f_w = S_f = S_T = 0$

Pr	SLM		bvp4c		Present	
	$f''(0)$	$-\theta'(0)$	$f''(0)$	$-\theta'(0)$	$f''(0)$	$-\theta'(0)$
1	0.87100777	0.42143140	0.81700776	0.42143144	0.81700776	0.42143144
10	0.54471433	0.88046306	0.54471423	0.88046307	0.54471422	0.88046307

Figure 2 Effects of Casson parameter on (a) velocity and (b) temperature profiles for different Λ and S_T, at $\Lambda_1 = 0.5$, $K = 0.5$, $Pr = 1$, $Ec = 1$, $M = 1$, $f_w = 0.5$, $S_f = 0.5$.

Figure 3 Effects of magnetic parameter on (a) velocity and (b) temperature profiles for different S_f and S_T, at $\Lambda_1 = 0.5$, $K = 0.5$, $Pr = 1$, $Ec = 1$, $f_w = 0.5$, $\Lambda = 0.5$, $\beta = 2$.

Figure 4 Effects of radiation parameter on (a) velocity and (b) temperature profiles for different S_f and S_T, at $\beta = 2$, $\Lambda_1 = 0.5$, $K = 0.5$, $Pr = 1$, $Ec = 1$, $M = 1$, $f_w = 0.5$, $\Lambda = 0.5$.

Figure 5 Effects of Λ_1 and *Ec* on (a) velocity and (b) temperature profiles for different f_w, at $\beta = 2$, $\Lambda = 0.5$, $K = 0.5$, $M = 1$, $K = 0.5$, $Pr = 1$, $S_T = 0.5$.

Figure 6 Skin friction coefficient *vs.* ξ for different S_f (a) and skin friction coefficient *vs.* ξ for different S_T (b) at $\beta = 2$, $\Lambda_1 = 0.5$, $K = 0.5$, $M = 1$, $Pr = 1$, $Ec = 1$, $f_w = 0.5$, $\Lambda = 0.5$.

Figure 7 Heat transfer coefficient *vs.* ξ for different S_f (a) and skin friction coefficient *vs.* ξ for different S_T (b) at $\beta = 2$, $\Lambda_1 = 0.5$, $K = 0.5$, $M = 1$, $Pr = 1$, $Ec = 1$, $f_w = 0.5$, $\Lambda = 0.5$.

Figure 8　Skin friction coefficient *vs. K* for different *S_f* (a) and skin friction coefficient *vs. ξ* for different *S_T* (b) at *β* = 2, *Λ_1* = 0.5, *M* = 1, *Pr* = 1, *Ec* = 1, *f_w* = 0.5, *Λ* = 0.5.

higher temperature profiles are noticed and lower temperature profiles are noticed in the presence of the thermal slip factor, as shown in Figure 2(b).

Figure 3 depicts the effect of the magnetic parameter M on the velocity and temperature profiles at different values of the velocity slip factor S_f in the case of velocity profiles (see Figure 3(a)), and thermal slip factor in the case of temperature profiles (see Figure 3(b)). M suppress velocity profiles. A magnetic field incident across a flowing fluid retards the velocity of the flow as noted in [4, 12]. The velocity profiles in the case of no-slip conditions resemble those of Narayana *et al.* [10]. It is noted that the velocity profiles are increased with the increase in the velocity slip factor as expected on a lubricated surface. In Figure 3(b) the temperature profiles are increased with increasing magnetic parameter and are decreased by the increase in the Forchheimer parameter Λ. Increasing the inertia causes more friction on the surface changing surface temperature, thereby causing the observed thermal slip.

Figure 4 shows the effect of the radiation parameter K on the velocity and temperature profiles at different values of the velocity slip factor S_f in the case of velocity profiles (see Figure 4(a)), and thermal slip factor in the case of temperature profiles (see Figure 4(b)). The same observation is noted in Figure 4(b); increasing K increases the temperature profiles.

Figure 5 illustrates the velocity response to the change in the Darcian drag force term Λ_1 at different values of the suction/injection parameter f_w (see Figure 5(a)), and the effect of the Eckert number Ec at different values of the suction/injection parameter f_w (see Figure 5(b)). In this case the Λ_1 is inversely proportional to the Darcy number, Da (also inversely proportional to the permeability of the medium). Increasing Λ_1 decreases the velocity profiles. It is noted that the case $f_w < 0$ (blowing) assists the flow, while the case $f_w > 0$ (suction) retards the velocity profiles. The differences of these results to those of Ramachandra *et al.* [1] are shown in the presence of a magnetic field which generally tend to suppress velocity profiles. The presence of viscous dissipation is also noted in the increase in the temperature profiles. In Figure 5(b) increasing the Eckert number results in the increase in the temperature profiles.

Figure 6 shows the plot of the skin friction coefficient *versus* ξ for different values of both the velocity slip factor S_f (see Figure 6(a)), and the thermal slip factor S_T (see Figure 6(b)). The skin friction coefficient decreases with increasing velocity slip factor and

also decreases with increasing ξ. In Figure 6(b) the skin friction coefficient decreases with increasing thermal slip factor.

Figure 7 shows the plot of the heat transfer coefficient *versus* ξ for different values of both the velocity slip factor S_f (see Figure 7(a)), and the thermal slip factor S_T (see Figure 7(b)). It is noted that, at the surface of the circle, there is a more significant change in heat transfer than further away from the surface of the circle. In Figure 7(b) increasing the velocity slip factor does not change the heat transfer at the surface. It is noticed that there is a large difference in the heat transfer further away from the circle surface.

Figure 8 shows the plot of the skin friction coefficient *versus* K for different values of both the velocity slip factor S_f (see Figure 8(a)), and the Nusselt number *versus* thermal slip factor S_T (see Figure 8(b)). In Figure 8(a) the skin friction coefficient increases with increasing thermal radiation K and decreases with increasing velocity slip factor, which is expected on a lubricated surface. There is a noticeable difference in the skin friction coefficient at different values of the velocity slip factor. In Figure 8(b) increasing the thermal radiation decreases the heat transfer coefficient. Increasing the thermal slip factor increases the heat transfer coefficient.

5 Conclusion
The study presented in this analysis of effects of radiation on MHD free convection of a Casson fluid from a horizontal circular cylinder with partial slip in non-Darcy porous medium with viscous dissipation provides numerical solutions for the boundary layer flow and heat transfer. The coupled nonlinear governing partial differential equations were solved using the bi-variate quasilinearization method (BQLM) and validated by the successive linearization method (SLM) and MATLAB's 'bvp4c'. This paper also describes the BQLM numerical method which uses collocation methods in both directions η (direction of increasing boundary layer thickness) and ξ (radial transpiration direction). The most important results are those reflected in the presence of a magnetic field and viscous dissipation in a Casson fluid, which were never reported before.

References
1. Ramachandra, PV, Subba, RA, Anwa, BO: Flow and heat transfer of Casson fluid from a horizontal cylinder with partial slip in non-Darcy porous medium. Appl. Comput. Math. **2**, 1-2 (2013)
2. Vajrravelu, K, Mukhopadhyay, S: Diffusion of chemically reactive species in Casson fluid flow over an unsteady permeable stretching surface. J. Hydrodyn. **25**, 591-598 (2013)
3. Mukhopadhyay, S, De, PR, Bhattacharyya, K, Layek, GC: Casson fluid flow over an unsteady stretching surface. Ain Shams Eng. J. **4** 933-938 (2013)
4. Nadeem, S, Ul Haq, R, Lee, C: MHD flow of a Casson fluid over an exponentially stretching sheet. Sci. Iran. **19**, 1550-1553 (2012)
5. Kameswaran, PK, Narayana, M, Makanda, G, Sibanda, P: On radiation effects on hydromagnetic Newtonian liquid flow due to an exponential stretching sheet. Bound. Value Probl. (2012). doi:10.1186/1687-2770-2012-105

6. Shateyi, S, Marewo, GT: Numerical analysis of MHD stagnation point flow of Casson fluid, heat and mass transfer over a stretching sheet. In: Balicki, J (ed.) Advances in Applied and Pure Mathematics, WSEAS, Proceedings of the 7th International Conference on Finite Diferences, Finite Elements, Finite Volumes, Boundary Elements (F-and-B '14), Gdansk, Poland, pp. 128-132 (2014). ISBN:978-960-474-380-3

7. Chamkha, AJ, Mujtaba, M, Quadri, A, Issa, C: Thermal radiation effects on MHD forced convection flow adjacent to a non-isothermal wedge in the presence of a heat source or sink. Heat Mass Transf. **39**, 305-312 (2003)

8. Pramanik, S: Casson fluid flow and heat transfer past an exponentially porous stretching surface in the presence of thermal radiation. Ain Shams Eng. J. **5**, 205-212 (2014)

9. Ece, CM: Free convection flow about a cone under mixed thermal boundary conditions and a magnetic field. Appl. Math. Model. **29**, 1121-1134 (2005)

10. Narayana, M, Awad, FG, Sibanda, P: Free magnetohydrodynamic flow and convection from a vertical spinning cone with cross diffusion effects. Appl. Math. Model. **37**, 2662-2678 (2013)

11. Nadeem, S, Ul Haq, R, Khan, ZH: Numerical study of MHD boundary layer flow of a Maxwell fluid past a stretching sheet in the presence of nanoparticles. J. Chin. Inst. Chem. Eng. **45**, 121-126 (2014)

12. Chen, CH: Combined heat and mass transfer in MHD free convection from a vertical surface with ohmic heating and viscous dissipation. Int. J. Eng. Sci. **42**, 699-713 (2004)

13. Anwa, I, Amin, N, Pop, I: Mixed convection boundary layer flow of a viscoelastic fluid over a horizontal circular cylinder. Int. J. Non-Linear Mech. **43**, 814-821 (2008)

14. Deka, RK, Paul, A, Chaliha, A: Transient free convection flow past an accelerated vertical cylinder in a rotating fluid. Ain Shams Eng. J. **5**, 505-513 (2014)

15. Ribeiro, VM, Coelo, PM, Pinho, FT, Alves, MA: Viscoelastic flow past a confined cylinder: three dimensional effects and stability. Chem. Eng. Sci. **111**, 364-380 (2014)

16. Patel, SA, Chhabra, RP: Steady flow of Bingham plastic fluids past an elliptical cylinder. J. Non-Newton. Fluid Mech. **165**, 32-53 (2013)

17. Awad, FG, Sibanda, P, Motsa, SS, Makinde, OD: Convection from an inverted cone in a porous medium with cross diffusion effect. Comput. Math. Appl. **61**, 1431-1441 (2011)

18. Hayat, T, Mustafa, M, Pop, I: Heat and mass transfer for Soret and Dufour's effect on mixed convection boundary layer flow over a stretching vertical surface in a porous medium filled with viscoelastic fluid. Commun. Nonlinear Sci. Numer. Simul. **15**, 1183-1196 (2010)

19. Cheng, CY: Soret and Dufour's effects on free convection boundary layer over a vertical cylinder in a saturated porous medium. Int. Commun. Heat Mass Transf. **37**, 796-800 (2010)

20. Chamkha, AJ, Rashad, AM: Natural convection from a vertical permeable cone in a nanofluid saturated porous media for uniform heat and nanoparticles volume fraction fluxes. Int. J. Numer. Methods Heat Fluid Flow **22**, 1073-1085 (2012)

21. Motsa, SS, Magagula, VM, Sibanda, P: A bivariate Chebyshev spectral collocation quasilinearization method for nonlinear parabolic equations. Sci. World J. (2014). doi:10.1155/2014/581987

22. Bellman, RE, Kalaba, RE: Quasilinearization and Nonlinear Boundary Value Problems. Elsevier, New York (1965)